

SPACE-BORNE CLOUD-NATIVE SATELLITE-DERIVED BATHYMETRY (SDB) MODELS USING ICESat-2 and SENTINEL-2

Nathan Marc Thomas^{1,1}, Avi Putri Pertiwi^{2,2}, Dimosthenis Traganos^{3,3}, David Lagomasino^{4,4}, Dimitris Poursanidis^{5,5}, Shalimar Giovanna Moreno^{6,6}, and Temilola Fatoyinbo^{7,7}

¹Earth System Science Interdisciplinary Center/NASA Goddard Space Flight Center

²German Aerospace Center (DLR)

³Deutsches Zentrum für Luft und Raumfahrt DLR Standort Berlin

⁴Coastal Studies Institute

⁵University of the Aegea, Foundation for Research and Technology Hellas, terraSolutions marine environment research

⁶Coastal Studies Institute, East Carolina University

⁷NASA GSFC

November 30, 2022

Abstract

Shallow nearshore coastal waters provide a wealth of societal, economic and ecosystem services, yet their topographic structure is poorly mapped due to a reliance upon expensive and time intensive methods. Space-borne bathymetric mapping has helped address these issues, but has remained dependent upon in situ measurements. Here we fuse ICESat-2 lidar data with Sentinel-2 optical imagery, within the Google Earth Engine geospatial cloud platform, to create wall-to-wall high-resolution bathymetric maps at regional-to-national scales in Florida, Crete and Bermuda. ICESat-2 bathymetric classified photons are used to train three Satellite Derived Bathymetry (SDB) methods, including Lyzenga, Stumpf and Support Vector Regression algorithms. For each study site the Lyzenga algorithm yielded the lowest RMSE (approx. 10-15%) when compared with in situ NOAA DEM data. We demonstrate a means of using ICESat-2 for both model calibration and validation, thus cementing a pathway for fully space-borne estimates of nearshore bathymetry in shallow, clear water environments.

Hosted file

thomas_etal_supporting_compressed.docx available at <https://authorea.com/users/561171/articles/608806-space-borne-cloud-native-satellite-derived-bathymetry-sdb-models-using-icesat-2-and-sentinel-2>

1 **SPACE-BORNE CLOUD-NATIVE SATELLITE-DERIVED BATHYMETRY (SDB) MODELS**
2 **USING ICESat-2 and SENTINEL-2**

3
4 **N. Thomas^{1,2}, A. P. Pertiwi³, D. Traganos³, D. Lagomasino⁴, D. Poursanidis⁵, S. Moreno⁴**
5 **and L. Fatoyinbo²**

6 ¹Earth System Science Interdisciplinary Center (ESSIC), University of Maryland, College Park,
7 MD USA

8 ²Biospheric Sciences Laboratory, NASA Goddard Space Flight Center, Greenbelt, MD USA

9 ³German Aerospace Center (DLR), Remote Sensing Technology Institute - Rutherfordstrasse 2,
10 12489 Berlin, Germany

11 ⁴Department of Coastal Studies, East Carolina University, Wanchese, NC, USA

12 ⁵Foundation for Research and Technology - Hellas (FORTH), Institute of Applied and
13 Computational Mathematics, N. Plastira 100, Vassilika Vouton, 70013 Heraklion, Greece

14 Corresponding author: Nathan Thomas (nathan.m.thomas@nasa.gov), Avi Putri Pertiwi
15 (avi.pertiwi@dlr.de)

16 **Key Points:**

- 17 • Nearshore bathymetric depths can be retrieved using ICESat-2 lidar data
- 18 • ICESat-2 bathymetric data can train Sentinel-2 Satellite Derived Bathymetry (SDB)
- 19 models at shoreline to national scales
- 20 • The fusion of ICESat-2 and Sentinel-2 data in the cloud paves the way for accurate
- 21 nearshore bathymetry mapping from space

23 Abstract

24 Shallow nearshore coastal waters provide a wealth of societal, economic and ecosystem services,
25 yet their topographic structure is poorly mapped due to a reliance upon expensive and time
26 intensive methods. Space-borne bathymetric mapping has helped address these issues, but has
27 remained dependent upon *in situ* measurements. Here we fuse ICESat-2 lidar data with Sentinel-
28 2 optical imagery, within the Google Earth Engine geospatial cloud platform, to create wall-to-
29 wall high-resolution bathymetric maps at regional-to-national scales in Florida, Crete and
30 Bermuda. ICESat-2 bathymetric classified photons are used to train three Satellite Derived
31 Bathymetry (SDB) methods, including Lyzenga, Stumpf and Support Vector Regression
32 algorithms. For each study site the Lyzenga algorithm yielded the lowest RMSE (approx. 10-
33 15%) when compared with *in situ* NOAA DEM data. We demonstrate a means of using ICESat-
34 2 for both model calibration and validation, thus cementing a pathway for fully space-borne
35 estimates of nearshore bathymetry in shallow, clear water environments.

36 **Plain Language Summary**

37 Knowledge of the depth of the shallow seafloor in coastal waters is needed for a wide range of
38 applications, including navigation and habitat monitoring. Mapping water depth in these
39 locations is expensive, arduous and sometimes dangerous. To overcome some of these
40 challenges, we used multiple satellite datasets to map water depth in several unique coastal
41 environments. ICESat-2 lidar data is able to sample the depth of the seabed along straight lines in
42 clear water and is then combined with other satellite imagery to derive wall-to-wall water depth
43 maps using well known regression algorithms. The results of these models are accurate maps of
44 water depth from space, containing a level of detail that can exceed some field collected
45 measurements.

46 **1 Introduction**

47 Accurate and current bathymetric maps are essential for informing coastal management
48 decision making. Emerging demands of the blue economy will open up new opportunities, but
49 could also have significant impacts on coastal regions and coastal habitats around the world
50 (LiVecci et al, 2019). Several key markets that will demand resources from the nearshore
51 environment have been identified for future and continued development including, marine
52 navigation, aquaculture, coastal resilience and disaster recovery, and isolated power supply.
53 Technological innovation that allows for contemporary nearshore and seafloor maps with regular
54 repeat observations will enable proper Marine Spatial Planning (MSP) and sharing of coastal
55 waters (Lester et al, 2018; Foley et al, 2010).

56 Competing sectors of the Blue Economy will change the bathymetry of nearshore
57 waterways and coastal regions in a variety of ways. Continued and new dredging to meet
58 shipping and navigation demands will increase channel depth and quantity of material spoil
59 (Bishop et al, 2006). Similarly, aquaculture practices such as kelp and oyster farming will reduce
60 erosion and increase sediment accumulation (Zhang et al, 2020; de Paiva et al, 2018). These
61 practices are predicted to change the structure of the seafloor which will have local-scale
62 implications for sub-aquatic ecosystems and nearshore navigation, by causing rapid changes in
63 benthic morphology. In addition, nearshore structure is increasingly being looked to as a source
64 of nature-based risk reduction solutions, including the use of natural barriers to sea level rise and
65 storm surges (Spalding et al, 2014). For improved coastal resilience assessments, accurate maps
66 of the seafloor are a critical parameter in measuring the wave attenuation of benthic habitats, like
67 seagrasses and coral reefs, (Narayan et al, 2016) and the erosion potential of dune-lined
68 beaches (Schweiger et al, 2020), but up-to-date and repeatable observations of sediment stability

69 (e.g. changes in water depth) and structural complexity are needed (Christianen et al, 2013:
70 Harris et al, 2018). These and other processes are not fully captured by current, openly available
71 coarse bathymetry data (Wolfl et al, 2019), which are limited in spatial and temporal resolution.
72 Increasing the resolutions of bathymetric data requires financial investment and substantial
73 energy expenditure to conduct more comprehensive or frequent surveys, particularly to capture
74 the detail required in the nearshore coastal environment.

75 Globally, there are several initiatives that procure bathymetric data collected by
76 hydrographic, oceanographic, and other vessels such as the International Hydrographic
77 Organization Data Centre for Digital Bathymetry (IHO DCDB; Marks, 2019), European Marine
78 Observation and Data Network (EMODnet; Emodnet, 2016), the Global Multi-Resolution
79 Topography (GMRT; Ryan et al, 2009) synthesis and the General Bathymetric Chart of the
80 Oceans (GEBCO; Kapoor, 1981). While these initiatives ensure that global bathymetric data are
81 available at satisfactory resolutions across large expanses of open ocean, these data are not
82 adequate for use in shallow waters where the vertical and spatial resolution is insufficient. With
83 high-resolution elevation data available for land surfaces (e.g., TanDEM-X; Wessel et al, 2018),
84 this leaves a corridor of missing data between the land and open ocean, where high quality data
85 are most required. Singlebeam (SBES) and Multibeam Echo Sounders (MBES) are commonly
86 deployed on small craft for local-scale high-resolution mapping (Janowski et al, 2018) but
87 collecting such data in shallow water can be hazardous and time consuming. Bathymetric lidar
88 data are well suited to fill this gap and can be acquired from airborne systems (Kim et al, 2017)
89 to circumvent navigation in busy shipping traffic, however they are economically expensive and
90 time-intensive to gather over large areas, particularly where frequent repeat surveys to capture
91 rapid changes are required.

92 Recent advances in Satellite-Derived Bathymetry (SDB) using multispectral Earth
93 Observations have lead to new methodological developments and applications through increased
94 spatial resolution and improved estimations (Traganos et al, 2018a; Caballero et al, 2019;
95 Caballero and Stumpf, 2020a, 2020b; Casal et al, 2019, 2020; Daly et al, 2020; Mateo-Perez et
96 al. 2020). Commercial satellite imagery has also been used to improve modeling on shallow
97 coastal bathymetry by achieving spatial resolutions of 3-m/pixel and daily revisits (Li et al,
98 2019; Poursanidis et al, 2019; Lyons et al, 2020). A number of SDB studies have improved water
99 depth retrieval through empirical correlations of surface reflectance with field-acquired depth
100 points (Lyzenga, 1978; Stumpf et al, 2003); machine learning that combines surface reflectance
101 and in-situ data (Pan et al, 2015; Geyman and Maloof, 2019; Albright and Glennie, 2020);
102 automatic tuning of SDB to water column conditions (Kerr and Purkis, 2018; Li et al, 2019);
103 inverting wave celerity based on the temporal offset between the satellite's bands (Daly et al,
104 2020) and physics-based inversion algorithms that produce highly-accurate SDB estimations but
105 at the expense of restricted scalability due to the required computational power for the inversion
106 (Casal et al, 2020). Despite the advances in SDB and the recent increased availability of cloud-
107 computing platforms such as the Google Earth Engine and Amazon Web Services, most
108 approaches still rely on airborne/shipborne data and local computing resources.

109 An ability to widely collect consistent SDB calibration and validation data will alleviate
110 some of the limitations in deriving routine nearshore bathymetry. The first release of ICESat-2
111 data highlighted the potential to acquire global bathymetric lidar data in shallow (<40m) coastal
112 waters (Markus et al, 2017; Parrish et al, 2019). This exciting new capability is especially timely
113 for coastal ecosystem studies as it paves the way for purely spaceborne SDB approaches in the
114 optically shallow global seascape realm (Albright and Glennie, 2020, Ma et al. 2020). Such

115 fusion approaches between satellite-based multispectral imagery and lidar data are now feasible
116 and could significantly reduce the needed time, costs, and computation to produce seamless SDB
117 maps, especially in data poor regions.

118 In the present study, we have developed one of the first fully space-based approaches to
119 measure nearshore bathymetry in optically shallow waters. The SDBs presented here are derived
120 from a newly designed cloud-native workflow within the Google Earth Engine cloud platform
121 (Gorelick et al, 2017) using multi-temporal Sentinel-2A/B data (Traganos et al, 2018a) and
122 ICESat-2 lidar observations (Parrish et al, 2019). Our primary aim is to evaluate the accuracy,
123 scalability and uncertainties of this approach for retrieving SDB, in comparison to freely available
124 bathymetric Digital Elevation Models (DEMs).

125 **2 Materials and Methods**

126 2.1 Data

127 2.1.1 ICESat-2

128 The Ice, Cloud and Elevation Satellite-2 (ICESat-2; IS-2) is a spaceborne altimeter launched in
129 September 2018. IS-2 carries the Advanced Topographic Laser Altimeter System (ATLAS)
130 which is a photon counting lidar, composed of three pairs of beams each separated by 3.3 km,
131 with 90 m between each pair. The pairs of lasers are divided into a strong and a weak beam,
132 based on a 1:4 energy ratio. Each laser has a repetition rate of 10 kHz with a wavelength of 532
133 nm. Each photon shot is separated by 70 cm with a footprint size of approximately 13 m. IS-2
134 geolocated photon data is provided in the ATL03 product which is disseminated through the
135 National Snow and Ice Data Center (NSIDC).

136 2.1.2 Sentinel-2

137 The estimation of satellite-derived bathymetry is based on Copernicus Sentinel-2 data and is
138 performed end-to-end within the Google Earth Engine (GEE) geospatial computing platform.
139 Sentinel-2 is a twin-satellite mission with 10-m spatial resolution and a 5-day revisit period and
140 which have provided open and free data since June 2015. In this study, we utilized both Level-
141 1C (L1C) top-of-atmosphere (TOA) reflectance (23 June 2015 - Present) and Level-2A (L2A)
142 atmospherically corrected surface reflectance (SR) (28 March 2017 - Present) datasets, available
143 within GEE.

144 2.1.3 Ancillary Bathymetric Data

145 2.1.3.1 NOAA Bathymetry

146 The Bermuda and Biscayne Bay, Florida topographic-bathymetric Digital Elevation models
147 (DEMs) were acquired from the NOAA National Centers for Environmental Information using
148 the Bathymetric Data Viewer portal (<https://maps.ngdc.noaa.gov/viewers/bathymetry/>). The
149 Bermuda DEM, at a resolution of 1 to 3 arc-second spatial resolution, was collected by multiple
150 institutions (e.g., Government of Bermuda, California State University, and NOAA) over a
151 period of 20 (1993-2012; Sutherland et al, 2013). Data was derived from a variety of
152 measurement techniques including topographic surveys, bathymetric lidar, gridded and raw
153 multibeam bathymetry, and nautical chart sounding depth, all combined to create a 1 arc-second
154 DEM. The Biscayne Bay (S200) DEM has a 1 arc-second spatial resolution which was derived
155 from nearly 150,000 soundings collected within the bay from 12 different surveys over a period
156 of 63 years (1930-1993; NOAA, 1998). The data was gridded by prioritizing more recent data
157 and/or highest resolution data over older and lower resolution data. Where data coverage was
158 sparse, generic interpolation and extrapolation models were used to fill gaps.

159

160 2.1.3.2 Singlebeam Sonar

161 Using low cost fishfinder tools, the collection of bathymetry data at the Gulf of Chania (Crete)
162 was completed June - July 2020 based on the method of Poursanidis et al (2018), covering a
163 depth range of 2 to 55 m.

164 2.2 Study Sites

165 2.2.1 Natura 2000 GR4340003, Crete

166 The Natura 2000 site GR4340003 is found on the North West of the the island of Crete, Greece.
167 The Island bounds the southern border of the Aegean Sea, approximately 160 km south of the

168 Greek mainland, and has an area of 8,336 km² and a coastline of 1,046 km. Specifically, the
169 Natura 2000 site GR4340003 “Chersonisos Rodopou – Paralia Maleme – Kolpos Chanion”
170 includes Rodopos peninsula and the coastal area from Kolympari to Platanias, at the NW part of
171 Crete, approximately 20 km from Chania city. The marine part of the site extends to a depth of
172 50 m and is characterized by the presence of *Posidonia oceanica* seagrass beds.

173 2.2.2 Biscayne Bay, Florida

174 Biscayne Bay is an estuary on the east coast of South Florida (USA) that is ecologically diverse
175 and serves as a nursery for many marine species. The bay is heavily influenced by human
176 activities such as boating, diving, recreational and commercial fishing, and serves as a major
177 shipping port. Around the major shipping port and private docks there are incised channels that
178 can exceed 15 m in depth and require regular dredging. The bay faces many ecological concerns
179 mostly due to declining water quality and freshwater inflows caused by increased runoff (Carey
180 et al, 2011). The benthic habitats of the central and southern regions of the bay are dominated by
181 seagrass, which includes *Thalassia testudinum*, with sporadic patch reef complexes (Lirman et
182 al, 2008).

183 2.2.3 Bermuda

184 Bermuda is a subtropical Caribbean Island over 1200 km north of the Bahamas, and 965 km east
185 of North Carolina. It is surrounded by the northernmost coral reef assemblage in the Atlantic
186 Ocean and also includes seagrass beds, mangroves, salt marshes, and rocky and sandy intertidal
187 areas (Coates et al, 2013). The reef complex forms a 2 to 10 m deep, 1.5 km wide rim that
188 surrounds the northern part of the islands. Patch reefs within the lagoon can be found within 1-2
189 m of the water surface. Marine transport is important to the island as most resources are imported

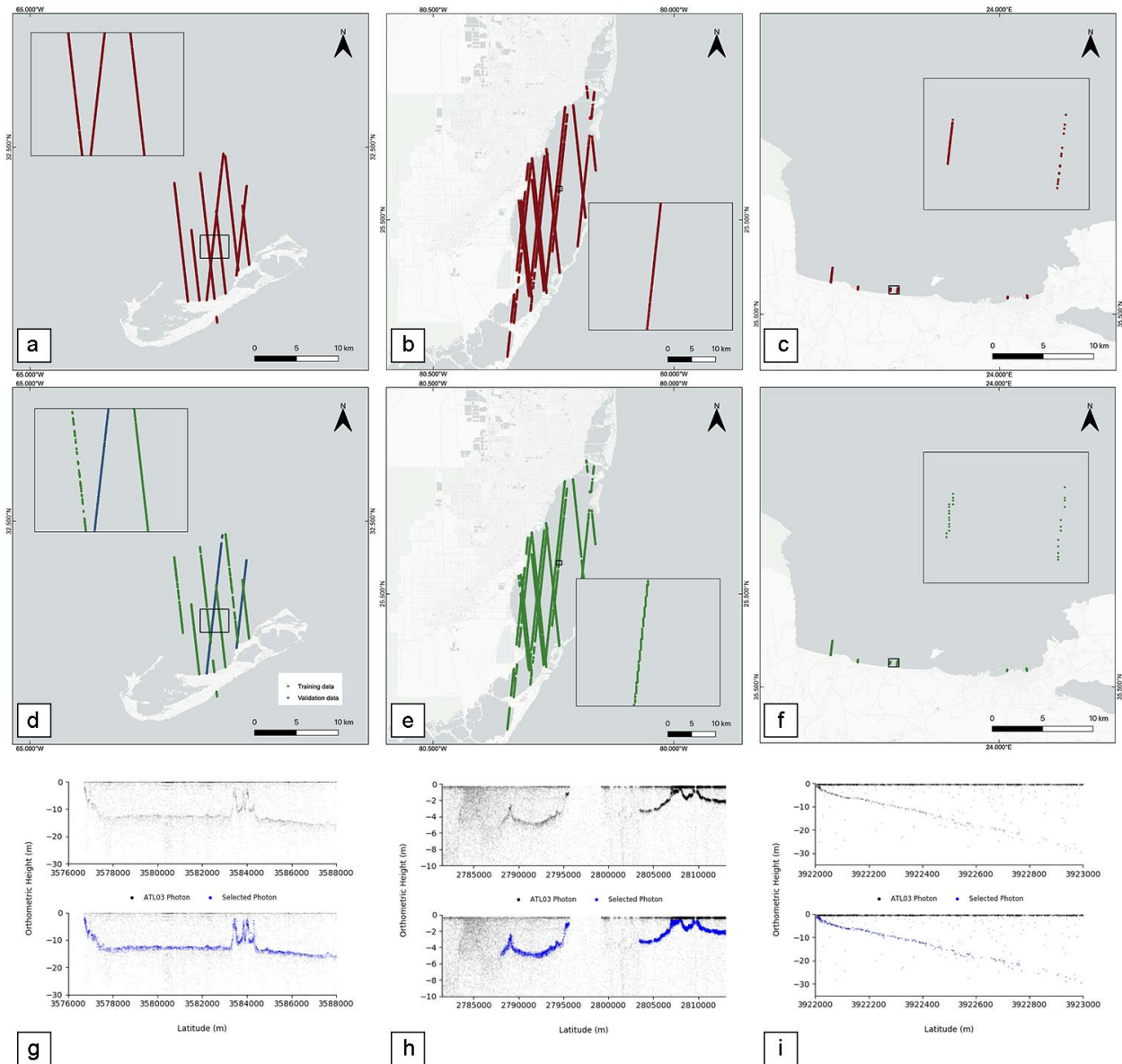
190 and shipping channels have been modified to accommodate large cruise ships. Channel dredging
191 has led to water quality issues in nearby regions (Lester et al, 2016).

192 2.3 Satellite-Derived Bathymetry Modeling

193 2.3.1 ICESat-2 Bathymetric Photons

194 ICESat-2 ATL03 data was queried via the Open Altimetry online portal
195 (<https://www.openaltimetry.org>) where it was subset and downloaded over our regions of interest
196 from the NSIDC server in HDF5 format (Figure 1, a, b, c). The ATL03 product does not record
197 the true location and elevation of sub-aquatic photons due to the refraction of the laser at the
198 air/water interface and the delayed travel time of the laser through the water column. To correct
199 the offset, accurate longitude, latitude, and photon height corrections were performed using the
200 methods of Parrish et al. (2019). This uses the spacecraft geometry and incident laser refraction
201 at the water surface to correct target photon depths, using inputs that include the IS-2 instrument
202 wavelength (532 nm), water salinity (35 Practical Salinity Units (PSU)) at atmospheric pressure
203 and location specific ocean temperatures. Photons were initially transformed to orthometric
204 height (EGM2008), and local UTM zone. Water surface photons were then manually selected
205 using an interactive python plot. The average of the selected water surface photons was defined
206 as the water surface model, from which photons below this were refraction corrected. Given that
207 the IS-2 data does not currently operate off-nadir pointing, longitude and latitude corrections
208 were minimal and photon depth correction was approximately 25% (at high precision) shallower
209 than the value recorded in the ATL03 data, in line with the calculations of Parrish et al (2019). A
210 bathymetric profile was manually selected from the corrected photons. Manual data selection
211 yielded a higher signal-to-noise ratio than trialled automated methods and ensured only high

212 quality depth information was collected. Examples of the refraction corrected photons and
 213 selected bathymetry photons are given in Figure 1 (g, h, i). For each IS-2 pass only the high-
 214 power beams were utilized. When input into the SDB model, only IS-2 depth photons with a
 215 system assigned “Land Confidence” level of 4 were used. These were aggregated into a Sentinel-
 216 2 10-m resolution grid (outlined below) and are shown in Figure 1 (d, e f).
 217



219 **Figure 1:** a, b & c) ICESat-2 depth data points for Bermuda, Biscayne Bay and Crete; d, e & f)
220 ICESat-2 depth data points with “Land Confidence” level 4 binned to Sentinel-2 10-m resolution
221 for Bermuda (SDB training (green) and validation (blue)), Biscayne Bay and Crete; g, h & i)
222 ICESat-2 photons and selected bathymetric profile for a single laser transect in Bermuda,
223 Biscayne Bay and Crete.

224

225

226 2.3.2 Sentinel-2 Sattelite Derived Bathymetry (SDB)

227

228 To pre-process and synthesize Sentinel-2 data to estimate and scale up the SDB models, we
229 developed a novel cloud-native geoprocessing workflow. This new cloud-based workflow builds
230 on the pre-processing and SDB estimation developed by Traganos et al, (2018a) and Traganos et
231 al, (2018b). Firstly, an evolved cloud mask was developed that combines the GEE-based
232 Sentinel-2 Cloud Probability dataset, the QA60 band, and metadata information. Next, a multi-
233 temporal mosaic was derived using four Sentinel-2 bands; B1-coastal aerosol, B2-blue, B3-
234 green, and B4-red, as these wavelengths are less susceptible to light attenuation. We derived the
235 mosaic using the 20th percentile for each study area data cube to reduce common natural
236 interferences in satellite images over coastal regions, such as sunglint, turbidity, waves, and
237 remaining clouds and haze.

238 After the initial pre-processing steps, three cloud-based SDB models were derived using the
239 relationship between the multi-temporal satellite data and the IS-2 data: i) a cluster-based linear
240 model merging a k-means unsupervised clustering algorithm (Arthur and Vassilvitskii, 2007)
241 with the algorithm of Lyzenga (1978)—hereafter CBL. This combination ensures that by

242 splitting the multi-temporal data into numerous classes, each reflectance band adheres to the
243 linear model assumption of homogeneous bottom albedo. This was particularly beneficial in
244 Bermuda and Biscayne Bay which have variable bottom types. Prior to selecting the relevant
245 bands for modeling, we performed preliminary statistical tests with various combinations of
246 Sentinel-2 bands with this method, and acquired the best accuracy with the multilinear regression
247 of B1, B2, B3, and B4. ii) a cluster-based ratio model applying the same k-means clustering
248 algorithm as above, prior to the ratio algorithm of Stumpf et al, (2003)—hereafter CBS. Both
249 CBL and CBS models follow the concept of the cluster-based regression (CBR) algorithm of
250 Geyman and Maloof (2019). Our preliminary statistical tests with various cluster-based ratios
251 identified the B3/B2 ratio as the most accurate model. It is also worth noting that the variable
252 benthic habitats in both Bermuda and Biscayne Bay prompted the use of five clusters in the CBL
253 and CBS SDB models. In contrast, Crete features a mainly homogeneous sandy seabed, averting
254 us from applying clustering prior to the empirical linear and ratio models which we applied and
255 tested here in their original form. iii) a machine learning model based on Support Vector
256 Regression (SVR)—hereafter SVR. We implemented an Epsilon-SVR with the default GEE
257 parameter and a linear kernel to map the first four log-transformed Sentinel-2 bands to a high-
258 dimensional feature space to fit a regression hyperplane. The relationship between IS-2 and
259 Sentinel-2 data, for the best performing model, at each study site is presented in Figure S1.

260

261 2.4 Reference Data and Accuracy Assessment

262 IS-2 data in all three study regions were used to train our three SDB models. We selected only
263 the IS-2 data points with a “Land Confidence” level of 4, within a Sentinel-2 10 m grid (Figure
264 1). Multiple IS-2 depths within a Sentinel-2 pixel were averaged. We used 80% of the IS-2

265 observations for training, using three different training/validation approaches for each study site,
266 driven by the availability and quality of reference bathymetric DEM data. A validation sample
267 size of 20% of the IS-2 dataset was used. For the country of Bermuda, we used six IS-2 transects
268 for training (5,173 points) and two IS-2 transects for validation—reduced from 2,510 to 1,293
269 points to fit the 80/20 ratio. Here, the training and validation data were collected on different
270 days, during different passes, which served as separate independent observations. Initial
271 comparison to a NOAA DEM yielded poor results due to the low temporal and spatial resolution
272 of the DEM (Figure S2 and Figure S3). For Biscayne Bay, IS-2 data was used for training
273 (34,342 points) whereas NOAA bathymetric DEM data was used for validation, using 8,585
274 (20%) random-stratified points. Lastly, an amalgamation of training with IS-2 data (133 points)
275 and with validation data collected from *in-situ* singlebeam data (85 points) was used in Crete.

276 For each validation, we calculated the root mean square error (RMSE) and mean absolute error
277 (MAE) as well as the standard deviation of the bathymetry estimation. Residual maps to identify
278 the spatial distribution of the differences between the SDB models and the corresponding NOAA
279 DEMs in Bermuda and Biscayne Bay were also generated (Figure S3 and Figure S4).

280 **3 Results**

281 The CBL method produced the most reliable SDB estimates at all sites with a RMSE of 2.62 m,
282 0.83 m, and 2.19 m, and MAE of 2 m, 0.65 m, and 2.02 m for Bermuda, Biscayne Bay, and
283 Crete, respectively. Among the three methods, SVR tends to underestimate the range of the
284 depths, although its error values do not differ much from that of the CBL method. The RMSEs of
285 the CBL models are lower or close to 10% of the maximum depth for the Bermuda (26 m) and
286 Crete (22 m) models, but close to 17% for the Biscayne Bay model where the maximum depth of

287 the modeled area is much lower (5 m). The variance of the models for Bermuda, Biscayne Bay,
 288 and Crete were 0.68, 0.79, and 0.83, respectively (Figure 2 j-l). The reference and the modeled
 289 depths of Bermuda (Figure 2 j) are in good agreement mostly between the depths of 11-17 m,
 290 whereas for the shallower Biscayne Bay (Figure 2 k) it is between 1.2-3 m.

291

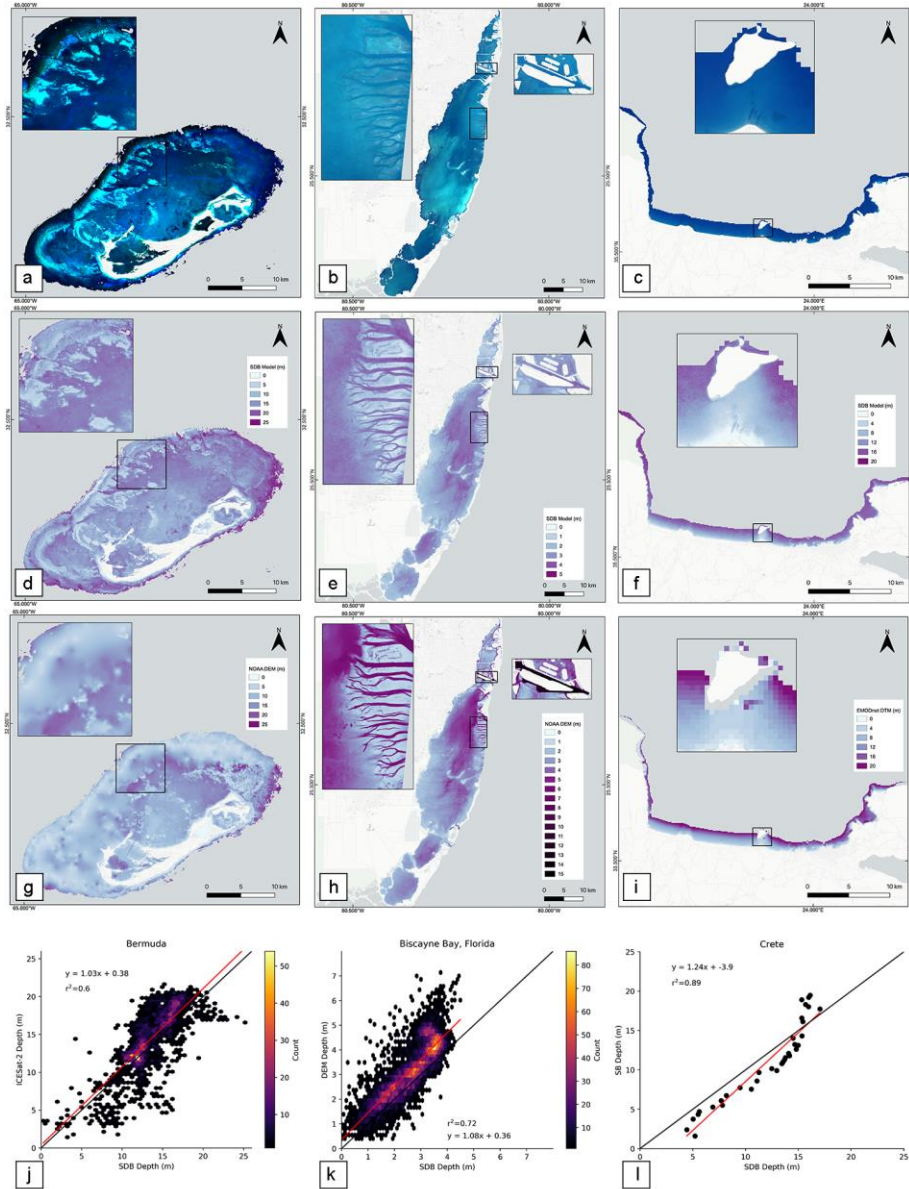
292

293 **Table 1:** Root mean square error, mean average error, and variance of the SDB model vs
 294 validation dataset in Bermuda, Biscayne Bay, and Crete

SITE	METHOD	RMSE (M)	MAE (M)	R ²	MAX DEPTH (M)*
BERMUDA	CBL	2.62	2.00	0.58	26
	CBS	2.89	2.21	0.50	26
	SVR	2.96	2.00	0.43	26
BISCAYNE BAY	CBL	0.83	0.65	0.72	5
	CBS	1.07	0.90	0.30	5
	SVR	0.89	0.73	0.64	5
CRETE	CBL	2.19	2.02	0.89	22
	CBS	2.41	2.18	0.85	22
	SVR	3.70	2.52	0.75	22

295 *based on the IS-2 training datasets

296



297

298

299 **Figure 2:** a, b, c) Sentinel-2 RGB synthesis. a) Bermuda: 53 L2A Surface Reflectance tiles, 597
 300 km² (March 28, 2017 – April 20, 2020); b) Biscayne Bay: 583 LIC Top-Of-Atmosphere tiles,
 301 689 km² (January 1, 2015 – December 31,2019); c) Crete: LIC 403LIC Top-Of-Atmosphere,
 302 61km² (January 1, 2015 – December 31,2019). d, e, f) CBL Bathymetry SDB at Bermuda,
 303 Biscayne Bay and Crete. g, h, i) NOAA DEM at Bermuda and Biscayne Bay and EMODnet at
 304 Crete, j, k, l) SDB-IS2 depth comparison at Bermuda, Biscayne Bay and Crete.

305 3.1 Comparison with publicly available DEM data

306 The detailed Bermuda SDB model picks up the bathymetric relief and rugosity of the shallow
307 and coral reef areas in more detail compared to the NOAA DEM product (Figure 2 d and g). The
308 Bermuda NOAA DEM product is a merge of multiple datasets and heavily interpolated in
309 sparsely covered region where navigation is difficult. For this reason, we observe high residuals
310 between the Bermuda SDB and NOAA DEM in the coral reef complexes (Figure 34). Similarly,
311 in shallow water regions, the Bermuda SDB model resolved the detailed relief of the seabed
312 which the NOAA DEM did not (Figure 2 h). With the variance of 0.14, the relationship between
313 SDB and NOAA DEM depths in Bermuda shows a very low agreement (Figure S2) specifically
314 at depths greater than 11 m. The mapped residuals range from -55.96 m to 51.28 m, where
315 negative values occur near patch reef complexes and positive values occur within the spur and
316 groove formations of the coral reef rim

317

318 In Biscayne Bay, the SDB model underestimates the depths of the navigation channels compared
319 to the Biscayne Bay NOAA DEM (Figure 2 e and h). More specifically, IS2 could not retrieve
320 the water depth in the deep dredged channels around the Miami Port (Figure 2 h), which reach a
321 depth of 17 m. The mapped residuals range from -14.11 m to 2.86 m (Figure S4). As the IS-2
322 photons are manually selected, it is noteworthy that photons were able to penetrate the water to
323 the depths of these channels, but did not exhibit an obvious surface for selection and were thus
324 omitted to avoid the use of incorrect depths in the model.

325

326 For the Crete study site, however, the SDB models under predict the deeper depths, specifically
327 greater than a depth of 15 m, where the water is optically deep. Here the relationship between IS-

328 2 reference depths and the log-transformed S-2 reflectance values become non-linear. The
329 reference and the modeled depths of Crete are in good agreement mostly between the depth of 7-
330 15 m. We obtained an available bathymetric map for the Crete study site for qualitative
331 comparison, but not for validation, from EMODNET, with a resolution of ~115 m (Figure 2 i).
332 The EMODnet bathymetry model has a reduced precision compared to the SDB and only
333 consists of integer values for each pixel. Compared to the EMODNET bathymetry map, our
334 Crete SDB model is in much higher spatial resolution (10 m), and features a more gradual
335 change of depths.

336 **4 Discussion and Conclusions**

337 In this study, we have demonstrated the unique fusion of ICESat-2 and Sentinel-2 data for
338 measuring coastal ecosystem structure and shallow water bathymetry, from coastline to country
339 scales. We developed adaptive bathymetry estimation methods derived solely from space-borne
340 observations over coastal waters in Bermuda, Biscayne Bay, and Crete at high-resolution and
341 with low error. The GEE cloud computing platform provides large computational power and a
342 well-integrated system to process hundreds of multi-temporal images in short time, as well as
343 perform analysis with thousands of data points with ease. The high resolution of Sentinel-2 and
344 ICESat-2 data allows us to map benthic variability in detail, improving upon available
345 bathymetry maps, especially within optically shallow water where the reflectance values between
346 different depths are more distinguishable.

347

348 We have demonstrated that our approach can yield products that are comparable to, and even
349 improve upon, locally collected existing data. At our study site locations, existing DEM data
350 were composed of multiple methods collected over a large temporal period at varying

351 resolutions. Therefore, changes in seabed structure due to hydrodynamic processes (such as
352 sediment deposition) and natural catastrophes could have been overlooked. At Biscayne Bay,
353 while our RSME error was small, some uncertainty can be attributed to differences between the
354 high resolution SDB model and lower temporal and spatial resolution NOAA DEM. However,
355 sources of uncertainty are also recognized in the remotely sensed data. At Biscayne Bay, IS-2
356 was unable to detect the bottom of dredged channels, which may have been caused by sediment
357 (turbidity in active shipping lanes) or the inability of the photons to reliably penetrate to those
358 depths. As the IS-2 bathymetric photons were manually selected, photons at these depths were
359 omitted as they did not form a coherent reflecting surface. While this limits the introduction
360 of noise into the model it also highlights potential sources of error that are introduced due to user
361 interpretation. This error may also be present in Bermuda and Crete, particularly where IS-2 was
362 used as both training and validation data. Furthermore, a more general source of uncertainty was
363 the effect of tide level in the analysis. By creating Sentinel-2 composite images using the 20%
364 percentile of tens to hundreds of tiles, we collected the darkest reflectance values, which might
365 not coincide with the depth values acquired by the IS-2 platform on a certain acquisition date.
366 The tidal range for our study sites was microtidal (< 1 m) thus the advantages of the approach
367 over the small introduction of error are interpreted to be an acceptable tradeoff.

368

369 The SDB models obtained with this approach are capable of contributing to the development of
370 the Blue Economy. Without the requirement for *in situ* data, repeat bathymetric maps can be
371 created for customized time-periods. This flexibility is required for monitoring changes in
372 nearshore topography for the purposes of navigation (Mavraeidopoulos et al, 2017), site
373 assessments, post-disaster mobilization and response (Stronko, 2013), infrastructure

374 developments (Coughlan et al, 2020), and for bathymetry and benthic cover mapping in regions
375 where field data acquisitions are scarce or prevented by a hazardous environment. Coastal zones
376 will experience a future increase in development and impacts from storm events (Horton et al,
377 2015) and therefore the need for contemporary and repeat bathymetric observations, particularly
378 for data poor regions, will be critical for ensuring sustainability of coastal resources. This is
379 particularly pertinent for “Big Ocean States” (or “Small Island Nations”) which may lack the
380 capacity to carry out bathymetric surveys of their territories (Purkis et al, 2019). A purely space-
381 borne cloud-based method empowers them to conduct their own structural and ecological
382 assessments.

383
384 Furthermore, our demonstrated method will allow the development of a global map of coastal
385 submerged ecosystems, which continues to be a critical need of the Blue Economy community.
386 This would be the foundation of global habitat accounting for currently poorly mapped sub-
387 aquatic ecosystems. Indeed, the need of global distribution maps for seagrasses, a blue carbon
388 ecosystem, has been an issue in coastal ecosystem studies, global conservation efforts and
389 national climate change policy agendas (Unsworth et al, 2019). We believe that by scaling up our
390 approach, we will be able to contribute one of the key factors in making a global map of
391 seagrass, and other shallow benthic habitats, possible.

392 **Acknowledgments, Samples, and Data**

393 The authors acknowledge the assistance of Christopher Parrish, Lori Magrider, Amy
394 Neuenschwander and Mike Alonzo for their guidance in correcting bathymetric ICESat-2
395 photons for the effects of refraction.

396

397 This research was funded by NASA Studies with ICESat-2 Program (Grant No.
398 80NSSC20K0968). Avi Putri Pertiwi and Dimosthenis Traganos acknowledge funding for their
399 efforts from the German Aerospace Center (DLR) through the Global Seagrass Watch project.
400 Dimitris Poursanidis acknowledges terraSolutions marine environment research for the support
401 in bathymetry data collection for the project “Coastal habitat mapping in support of conservation
402 activities for the loggerhead *Caretta caretta*” funded by MEDPAN.

403

404 Datasets are available at: <https://doi.org/10.6084/m9.figshare.13017209.v1>

405

406 **References**

407

408 Albright, A. and Glennie, C., 2020. Nearshore Bathymetry From Fusion of Sentinel-2 and
409 ICESat-2 Observations. *IEEE Geoscience and Remote Sensing Letters*.

410

411 Arthur, D. and Vassilvitskii, S., k-means++: The Advantages of Careful Seeding, SODA’07
412 Proceedings of the eighteenth annual ACM-SIAM symposium on Discrete algorithms, New
413 Orleans, Louisiana, 2007. URL <https://theory.stanford.edu/~sergei/papers/kMeansPP-soda.pdf>, pp.1027-1035.

415

416 Lyons, M., M. Roelfsema, C., V. Kennedy, E., M. Kovacs, E., Borrego-Acevedo, R., Markey,
417 K., Roe, M., M. Yuwono, D., L. Harris, D., R. Phinn, S. and Asner, G.P., 2020. Mapping the
418 world's coral reefs using a global multiscale earth observation framework. *Remote Sensing in
419 Ecology and Conservation*.

420

421 Bishop, M.J., Peterson, C.H., Summerson, H.C., Lenihan, H.S. and Grabowski, J.H., 2006.
422 Deposition and long-shore transport of dredge spoils to nourish beaches: impacts on benthic
423 infauna of an ebb-tidal delta. *Journal of Coastal Research*, 22(3 (223)), pp.530-546.

424

425 Caballero, I. and Stumpf, R.P., 2020a. Atmospheric correction for satellite-derived bathymetry in
426 the Caribbean waters: from a single image to multi-temporal approaches using Sentinel-
427 2A/B. *Optics Express*, 28(8), pp.11742-11766.

428

429 Caballero, I. and Stumpf, R.P., 2020b. Towards routine mapping of shallow bathymetry in
430 environments with variable turbidity: contribution of Sentinel-2A/B satellites mission. *Remote*
431 *Sensing*, 12(3), p.451.

432

433 Caballero, I., Stumpf, R.P. and Meredith, A., 2019. Preliminary assessment of turbidity and
434 chlorophyll impact on bathymetry derived from Sentinel-2A and Sentinel-3A satellites in South
435 Florida. *Remote Sensing*, 11(6), p.645.

436

437 Carey, R.O., Migliaccio, K.W., Li, Y., Schaffer, B., Kiker, G.A. and Brown, M.T., 2011. Land
438 use disturbance indicators and water quality variability in the Biscayne Bay Watershed,
439 Florida. *Ecological Indicators*, 11(5), pp.1093-1104.

440

- 441 Casal, G., Harris, P., Monteys, X., Hedley, J., Cahalane, C. and McCarthy, T., 2020.
442 Understanding satellite-derived bathymetry using Sentinel 2 imagery and spatial prediction
443 models. *GIScience & Remote Sensing*, 57(3), pp.271-286.
444
- 445 Casal, G., Hedley, J.D., Monteys, X., Harris, P., Cahalane, C. and McCarthy, T., 2020. Satellite-
446 derived bathymetry in optically complex waters using a model inversion approach and Sentinel-2
447 data. *Estuarine, Coastal and Shelf Science*, p.106814.
448
- 449 Christianen, M.J., van Belzen, J., Herman, P.M., van Katwijk, M.M., Lamers, L.P., van Leent,
450 P.J. and Bouma, T.J., 2013. Low-canopy seagrass beds still provide important coastal protection
451 services. *PloS one*, 8(5), p.e62413.
452
- 453 Coates, K.A., Fourqurean, J.W., Kenworthy, W.J., Logan, A., Manuel, S.A. and Smith, S.R.,
454 2013. Introduction to Bermuda: geology, oceanography and climate. In *Coral reefs of the United*
455 *Kingdom overseas territories* (pp. 115-133). Springer, Dordrecht.
456
- 457 Coughlan, M., Long, M. and Doherty, P., 2020. Geological and geotechnical constraints in the
458 Irish Sea for offshore renewable energy. *Journal of Maps*, 16(2), pp.420-431.
459
- 460 Daly, C.J., Baba, W., Bergsma, E., Almar, R. and Garlan, T., 2020. The New Era of Regional
461 Coastal Bathymetry from Space: A Showcase for West Africa using Sentinel-2 Imagery.
462

463 de Paiva, J.N.S., Walles, B., Ysebaert, T. and Bouma, T.J., 2018. Understanding the
464 conditionality of ecosystem services: The effect of tidal flat morphology and oyster reef
465 characteristics on sediment stabilization by oyster reefs. *Ecological Engineering*, 112, pp.89-95.
466

467 EMODnet Bathymetry Consortium, 2016. EMODnet Digital Bathymetry (DTM 2016).
468

469 Foley, M.M., Halpern, B.S., Micheli, F., Armsby, M.H., Caldwell, M.R., Crain, C.M., Prahler,
470 E., Rohr, N., Sivas, D., Beck, M.W. and Carr, M.H., 2010. Guiding ecological principles for
471 marine spatial planning. *Marine policy*, 34(5), pp.955-966.
472

473 Geyman, E.C. and Maloof, A.C., 2019. A simple method for extracting water depth from
474 multispectral satellite imagery in regions of variable bottom type. *Earth and Space Science*, 6(3),
475 pp.527-537.
476

477 Gorelick, N., Hancher, M., Dixon, M., Ilyushchenko, S., Thau, D. and Moore, R., 2017. Google
478 Earth Engine: Planetary-scale geospatial analysis for everyone. *Remote sensing of*
479 *Environment*, 202, pp.18-27.
480

481 Harris, D.L., Rovere, A., Casella, E., Power, H., Canavesio, R., Collin, A., Pomeroy, A.,
482 Webster, J.M. and Parravicini, V., 2018. Coral reef structural complexity provides important
483 coastal protection from waves under rising sea levels. *Science Advances*, 4(2), p.eaao4350.
484

485 Horton, R., Little, C., Gornitz, V., Bader, D. and Oppenheimer, M., 2015. New York City Panel
486 on Climate Change 2015 report chapter 2: Sea level rise and coastal storms. *Annals of the New*
487 *York Academy of Sciences*, 1336(1), pp.36-44.

488

489 Janowski, L., Trzcinska, K., Tegowski, J., Kruss, A., Rucinska-Zjadacz, M. and Pocwiardowski,
490 P., 2018. Nearshore benthic habitat mapping based on multi-frequency, multibeam echosounder
491 data using a combined object-based approach: A case study from the Rowy site in the southern
492 Baltic sea. *Remote Sensing*, 10(12), p.1983.

493

494 Kapoor, D.C., 1981. General bathymetric chart of the oceans (GEBCO). *Marine Geodesy*, 5(1),
495 pp.73-80.

496

497 Kerr, J.M. and Purkis, S., 2018. An algorithm for optically-deriving water depth from
498 multispectral imagery in coral reef landscapes in the absence of ground-truth data. *Remote*
499 *Sensing of Environment*, 210, pp.307-324.

500

501 Kim, H., Lee, S.B. and Min, K.S., 2017. Shoreline change analysis using airborne LiDAR
502 bathymetry for coastal monitoring. *Journal of Coastal Research*, (79), pp.269-273.

503

504 Lester, S.E., White, C., Mayall, K. and Walter, R.K., 2016. Environmental and economic
505 implications of alternative cruise ship pathways in Bermuda. *Ocean & Coastal*
506 *Management*, 132, pp.70-79.

507

508 Li, J., Knapp, D.E., Schill, S.R., Roelfsema, C., Phinn, S., Silman, M., Mascaro, J. and Asner,
509 G.P., 2019. Adaptive bathymetry estimation for shallow coastal waters using Planet Dove
510 satellites. *Remote Sensing of Environment*, 232, p.111302.

511

512 Lirman, D., Deangelo, G., Serafy, J., Hazra, A., Hazra, D.S., Herlan, J., Luo, J., Bellmund, S.,
513 Wang, J. and Clausing, R., 2008. Seasonal changes in the abundance and distribution of
514 submerged aquatic vegetation in a highly managed coastal lagoon. *Hydrobiologia*, 596(1), p.105.

515

516 LiVecchi, A., Copping, A., Jenne, D., Gorton, A., Preus, R., Gill, G., Robichaud, R., Green, R.,
517 Geerlofs, S., Gore, S. and Hume, D., 2019. Powering the blue economy; exploring opportunities
518 for marine renewable energy in maritime markets. *US Department of Energy, Office of Energy*
519 *Efficiency and Renewable Energy. Washington, DC*, p.207.

520

521 Lyzenga, D.R., 1985. Shallow-water bathymetry using combined lidar and passive multispectral
522 scanner data. *International Journal of Remote Sensing*, 6(1), pp.115-125.

523

524 Ma, Y., Xu, N., Liu, Z., Yang, B., Yang, F., Wang, X.H. and Li, S., 2020. Satellite-derived
525 bathymetry using the ICESat-2 lidar and Sentinel-2 imagery datasets. *Remote Sensing of*
526 *Environment*, 250, p.112047.

527

528 Marks, K., 2019. The IHO-IOC GEBCO Cook Book.

529

- 530 Mateo-Pérez, V., Corral-Bobadilla, M., Ortega-Fernández, F. and Vergara-González, E.P., 2020.
531 Port Bathymetry Mapping Using Support Vector Machine Technique and Sentinel-2 Satellite
532 Imagery. *Remote Sensing*, 12(13), p.2069.
- 533
- 534 Mavraeidopoulos, A.K., Pallikaris, A. and Oikonomou, E., 2017. Satellite derived bathymetry
535 (SDB) and safety of navigation. *The International Hydrographic Review*.
- 536
- 537 Markus, T., Neumann, T., Martino, A., Abdalati, W., Brunt, K., Csatho, B., Farrell, S., Fricker,
538 H., Gardner, A., Harding, D. and Jasinski, M., 2017. The Ice, Cloud, and land Elevation
539 Satellite-2 (ICESat-2): science requirements, concept, and implementation. *Remote Sensing of*
540 *Environment*, 190, pp.260-273.
- 541
- 542 Narayan, S., Beck, M.W., Reguero, B.G., Losada, I.J., Van Wesenbeeck, B., Pontee, N.,
543 Sanchirico, J.N., Ingram, J.C., Lange, G.M. and Burks-Copes, K.A., 2016. The effectiveness,
544 costs and coastal protection benefits of natural and nature-based defences. *PloS one*, 11(5),
545 p.e0154735.
- 546
- 547 NOAA. 1998. Biscayne Bay, FL (S200) Bathymetric Digital Elevation Model(30 meter
548 resolution) Derived From Source Hydrographic Survey Soundings Collected by NOAA
- 549
- 550 Pan, Z., Glennie, C., Legleiter, C. and Overstreet, B., 2015. Estimation of water depths and
551 turbidity from hyperspectral imagery using support vector regression. *IEEE Geoscience and*
552 *Remote Sensing Letters*, 12(10), pp.2165-2169.

553

554 Parrish, C.E., Magruder, L.A., Neuenschwander, A.L., Forfinski-Sarkozi, N., Alonzo, M. and
555 Jasinski, M., 2019. Validation of ICESat-2 ATLAS bathymetry and analysis of ATLAS's
556 bathymetric mapping performance. *Remote Sensing*, *11*(14), p.1634.

557

558 Poursanidis, D., Topouzelis, K. and Chrysoulakis, N., 2018. Mapping coastal marine habitats and
559 delineating the deep limits of the Neptune's seagrass meadows using very high resolution Earth
560 observation data. *International journal of remote sensing*, *39*(23), pp.8670-8687.

561

562 Poursanidis, D., Traganos, D., Chrysoulakis, N. and Reinartz, P., 2019. Cubesats allow high
563 spatiotemporal estimates of satellite-derived bathymetry. *Remote Sensing*, *11*(11), p.1299.

564

565 Purkis, S.J., Gleason, A.C., Purkis, C.R., Dempsey, A.C., Renaud, P.G., Faisal, M., Saul, S. and
566 Kerr, J.M., 2019. High-resolution habitat and bathymetry maps for 65,000 sq. km of Earth's
567 remotest coral reefs. *Coral Reefs*, *38*(3), pp.467-488.

568

569 Ryan, W.B., Carbotte, S.M., Coplan, J.O., O'Hara, S., Melkonian, A., Arko, R., Weissel, R.A.,
570 Ferrini, V., Goodwillie, A., Nitsche, F. and Bonczkowski, J., 2009. Global multi-resolution
571 topography synthesis. *Geochemistry, Geophysics, Geosystems*, *10*(3).

572

573 Schweiger, C., Koldrack, N., Kaehler, C. and Schuettrumpf, H., 2020. Influence of Nearshore
574 Bathymetry Changes on the Numerical Modelling of Dune Erosion. *Journal of Coastal
575 Research*, *36*(3), pp.545-558.

576

577 Spalding, M.D., Ruffo, S., Lacambra, C., Meliane, I., Hale, L.Z., Shepard, C.C. and Beck, M.W.,
578 2014. The role of ecosystems in coastal protection: Adapting to climate change and coastal
579 hazards. *Ocean & Coastal Management*, 90, pp.50-57.

580

581 Stronko, J.M., 2013. *Hurricane Sandy Science Plan—Coastal Topographic and Bathymetric*
582 *Data to Support Hurricane Impact Assessment and Response* (No. 2013-3099). US Geological
583 Survey.

584

585 Stumpf, R.P., Holderied, K. and Sinclair, M., 2003. Determination of water depth with high-
586 resolution satellite imagery over variable bottom types. *Limnology and*
587 *Oceanography*, 48(1part2), pp.547-556.

588

589 Sutherland, M.G., McLean, S.J., Love, M.R., Carignan, K.S. and Eakins, B.W., 2014. Digital
590 Elevation Models of Bermuda: Data Sources, Processing and Analysis. *Boulder, CO: NOAA*
591 *National Geophysical Data Center, US Dept. of Commerce*, 7.

592

593 Traganos, D., Poursanidis, D., Aggarwal, B., Chrysoulakis, N. and Reinartz, P., 2018a.
594 Estimating satellite-derived bathymetry (SDB) with the google earth engine and sentinel-
595 2. *Remote Sensing*, 10(6), p.859.

596

597 Traganos, D., Aggarwal, B., Poursanidis, D., Topouzelis, K., Chrysoulakis, N. and Reinartz, P.,
598 2018b. Towards global-scale seagrass mapping and monitoring using Sentinel-2 on Google Earth
599 Engine: The case study of the aegean and ionian seas. *Remote Sensing*, 10(8), p.1227.

600

601 Unsworth, R.K., McKenzie, L.J., Collier, C.J., Cullen-Unsworth, L.C., Duarte, C.M., Eklöf, J.S.,
602 Jarvis, J.C., Jones, B.L. and Nordlund, L.M., 2019. Global challenges for seagrass
603 conservation. *Ambio*, 48(8), pp.801-815.

604

605 Wessel, B., Huber, M., Wohlfart, C., Marschalk, U., Kosmann, D. and Roth, A., 2018. Accuracy
606 assessment of the global TanDEM-X Digital Elevation Model with GPS data. *ISPRS Journal of*
607 *Photogrammetry and Remote Sensing*, 139, pp.171-182.

608

609 Wöfl, A.C., Snaith, H., Amirebrahimi, S., Devey, C.W., Dorschel, B., Ferrini, V., Huvenne,
610 V.A., Jakobsson, M., Jencks, J., Johnston, G. and Lamarche, G., 2019. Seafloor Mapping—the
611 challenge of a truly global ocean bathymetry. *Frontiers in Marine Science*, 6, p.283.

612

613 Zhang, Z., Huang, H., Liu, Y., Bi, H. and Yan, L., 2020. Numerical study of hydrodynamic
614 conditions and sedimentary environments of the suspended kelp aquaculture area in Heini
615 Bay. *Estuarine, Coastal and Shelf Science*, 232, p.106492.

616